ISSN 1063-7788, Physics of Atomic Nuclei, 2015, Vol. 78, No. 5, pp. 557–573. © Pleiades Publishing, Ltd., 2015.
Original Russian Text © B.S. Ishkhanov, V.N. Orlin, 2015, published in Yadernaya Fizika, 2015, Vol. 78, Nos. 7-8, pp. 601–617.

NUCLEI
Theory

Modified Version of the Combined Model of Photonucleon Reactions

B. S. Ishkhanov[1),2)] and V. N. Orlin[2)*]

Received December 11, 2014

Abstract—A refined version of the combined photonucleon-reaction model is described. This version makes it possible to take into account the effect of structural features of the doorway dipole state on photonucleon reactions in the energy range of $E_\gamma \lesssim 30$ MeV. In relation to the previous version of the model, the treatment of isospin effects at the preequilibrium and evaporation reaction stages is refined; in addition, the description of the semidirect effect caused by nucleon emission from the doorway dipole state is improved. The model in question is used to study photonucleon reactions on the isotopes $^{35-56}$Ca and $^{102-134}$Sn in the energy range indicated above.

DOI: 10.1134/S1063778815040067

1. INTRODUCTION

In accordance with Bohr's postulate [1], it is assumed in the combined photonucleon-reaction model that a nuclear reaction can approximately be broken down into two independent stages: the formation of a compound system and the decay of this system into reaction products. In addition, it is assumed in this model that, in the mass range extending from values around $A \sim 40$ to A values corresponding to transuranium elements, an analysis can be restricted to considering only three competing channels of decay of the compound system. These are the neutron, proton, and photon channels.

Up to the pion-production threshold, photoabsorption on a nucleus is determined by photon interaction only with one- and two-nucleon nuclear currents [2, 3]. In the first case, only one nucleon is excited upon photon absorption. This is a dominant process in the region of low energies ($E_\gamma \lesssim 40$ MeV), where the interaction of electromagnetic radiation with a nucleus leads to the formation of giant resonances [the giant dipole resonance (GDR) is the main one among them], which are a coherent mixture of one-particle–one-hole ($1p1h$) excitations. The quasideuteron (QD) photoabsorption mechanism becomes dominant above this region. Within this mechanism, the excited nucleon exchanges a virtual pion with the neighboring nucleon. As a result, the energy and momentum of the absorbed photon are transferred to a correlated proton–neutron pair rather to a single nucleon.

In describing giant resonances, use is most frequently made of various versions of the $1p1h$ approximation of the shell model—for example, the random-phase approximation (RPA) [4], the theory of finite Fermi systems (TFFS) [5], and the coupled-channel method [6]. Despite the difference in substantiations, all of them lead to nearly identical results. For a reasonable choice of residual forces, these calculations reproduce by and large satisfactorily the mean energies and the sums of oscillator strengths of giant resonances in medium-mass and heavy nuclei. However, they run into serious difficulties in describing the structure and decay features of giant resonances. In the most advanced calculations of giant resonances, $2p2h$ states are therefore taken into account in addition to $1p1h$ configurations (see, for example, the TFFS calculations in [7, 8] for closed-shell medium-mass and heavy nuclei and the calculations of photonuclear reactions for the ^{89}Y, ^{140}Ce, and ^{208}Pb nuclei in [9], where spreading effects were included phenomenologically).

However, the problem of constructing a detailed description of the formation and decay of giant resonances has so far remained by and large unresolved because of limitations of the particle–hole approach. As a matter of fact, this approach can be used in describing giant resonances only in those cases where the ground state of the nucleus being considered does not differ very strongly from the particle–hole or quasiparticle physics vacuum. Therefore, it comes as no surprise that the most realistic microscopic calculations were performed for magic and nearly magic nuclei. For this reason, a simple semimicroscopic approach [10, 11] is used in the combined

1)Faculty of Physics, Moscow State University, Moscow, 119991 Russia.
2)Skobeltsyn Institute of Nuclear Physics, Moscow State University, Moscow, 119991 Russia.
*E-mail: orlinvn@yandex.ru

photonucleon-reaction model to describe giant resonances. This approach, supplemented with phenomenological data, makes it possible to describe the gross structure of giant resonances for the majority of medium-mass and heavy nuclei. The quasideuteron component of the photoabsorption cross section can be found with the aid of the Levinger quasideuteron model [12, 13].

In the past decade, much attention has been given to considering high-energy resonances, the majority of them being overtones of lower lying basic resonances [14–18]. The combined photonucleon-reaction model takes into account two such resonances—the isovector quadrupole resonance and the overtone of the giant dipole resonance—which make a sizable contribution to photonucleon reactions in the energy range of 20–40 MeV.

In describing nucleon and photon emission, which is the reaction stage following photoabsorption, one usually employs semiclassical statistical models (exciton [19–22] and hybrid [23–27] models) and quantum multistep preequilibrium models [28–30] combined with the Weisskopf–Ewing evaporation model. Quantum models, in which the nucleon-emission probability is determined in terms of quantum-mechanical transition amplitudes, describe the angular distribution of reaction products better than semiclassical models. However, this drawback of semiclassical models is compensated to a considerable extent by the simplicity of their application and by their high predictive power in describing the nucleon energy spectra and total reaction cross sections. For these reasons, they are still widely used in specific calculations [31, 32].

At the same time, the use of semiclassical preequilibrium models entails difficulties in describing photonuclear reactions at energies in the range of $E \lesssim 30$ MeV, because a powerful collectivized dipole state that arises as a coherent superposition of various $1p1h$ excitations appears to be the doorway state in this region. This circumstance is usually disregarded. However, this leads to serious errors in estimating the relative yield of photoneutrons and photoprotons and in describing their energy spectra.

In order to describe correctly the competition of the neutron and proton channels of the decay of a giant dipole resonance, it is necessary to take into account its isospin splitting into the $T_<$ and $T_>$ components, since, by virtue of isospin conservation, the $T_>$ component decays predominantly through the proton channel (in $N > Z$ nuclei) or through the neutron channel (in $Z > N$ nuclei). Without allowance for this circumstance, it is not possible to describe correctly the photonucleon yield either from comparatively light nuclei (of mass number in the range of $A \sim 40$–50), where the $T_>$ component of the giant dipole resonance is significant, or from heavy nuclei, where, despite the smallness of this component, it serves as a dominant source of photoprotons.

It should also be borne in mind that, within the preequlibrium models considered in [19–27], semidirect photonucleon reactions are treated as nucleon emission from the $1p1h$ doorway state. Concurrently, it is assumed that, at a given excitation energy, all $1p1h$ configurations are populated with equal probabilities, and the effect of the orbital angular (l) and total angular (j) momenta of an excited nucleon on its ability to leave the target nucleus is disregarded. This disregard of the doorway-state shell structure entails an incorrect treatment of the semidirect photoeffect (excited-nucleon emission directly from the doorway state) and leads to especially important consequences in describing the photodisintegration of light and medium-mass nuclei, in which case semidirect reactions generate a significant fraction of emitted photonucleons.

These issues were considered in [33, 34] on the basis of earlier versions of the combined photonucleon-reaction model. However, the relations obtained there disregard special features of $A < 50$ nuclei; therefore, it is legitimate to use them only in describing photonuclear reactions on medium-mass and heavy nuclei.

In the present study, we consider in detail the problem of taking into account isospin effects within the statistical approach. This will permit to do this in comparatively light nuclei. Moreover, the effect of various $1p1h$ configurations of the doorway state on its decay properties is taken into account in terms of the nucleon transmission coefficients T_{jl} rather than within R-matrix theory (as was done earlier), which are calculated on the basis of the optical model. This improves substantially the reliability of the results.

The ensuing exposition is organized as follows. In Section 2, we briefly outline our procedure for calculating the photoabsorption cross section. In Section 3, we consider a scheme for calculating total cross sections for multiparticle photonucleon reactions and photonucleon spectra integrated with respect to the angles. Corrections that must be introduced in semiclassical statistical models in order to take into account the impact of isospin effects on photonucleon reactions are discussed in Section 4. The photon decay channel is considered in Section 5. A procedure for taking into account the effect of the structure of the doorway dipole state on the semidirect photoeffect is described in Section 6. In Section 7, the model formulated in this study is applied to describing photonucleon reactions on the isotopes $^{35-56}$Ca and $^{116-128}$Sn in the energy range of $E_\gamma \lesssim 30$ MeV. The basic results of this study are listed in Section 8.

2. PHOTOABSORPTION CROSS SECTION

Upon disregarding threshold effects, the total photoabsorption cross section can approximately be represented in the form

$$\sigma_{\text{abs}}(E_\gamma) \approx \sum_s \sigma_s(E_\gamma) \quad (1)$$

$$\approx \sum_{s\neq\text{QD}} \frac{2}{\pi} \frac{\sigma_{\text{int}}(s)E_\gamma^2\Gamma_s}{(E_\gamma^2 - E_s^2)^2 + E_\gamma^2\Gamma_s^2} + \sigma_{\text{QD}}(E_\gamma),$$

where the index s corresponds to various components of the photoabsorption cross section, which are associated with various giant resonances—the dipole one, the quadrupole one, and the overtone of the giant dipole resonance (which are approximated by one or several Lorentzian curves, depending on their structure)—as well as ($s = \text{QD}$) with quasideuteron photoabsorption [12, 13].

For the resonance curves, the energies E_s and integrated cross sections $\sigma_{\text{int}}(s)$ are calculated on the basis of a semimicroscopic model of vibrations (see [11, 34, 35]). The widths G_s of these resonances are estimated either with the aid of the exciton model or, in the case of a dipole resonance, with the aid of the respective semiempirical formula obtained in [36] from an analysis of experimental data.

3. PHOTONUCLEON CROSS SECTIONS AND SPECTRA

In the exciton model, it is assumed that, after photon absorption, there arises a doorway state featuring $m = m_0$ excitons ($m_0 = 2$ for giant resonances that are $1p1h$ excitations, and $m_0 = 4$ for a quasideuteron $2p2h$ excitation). This primary excitation decays via excited-nucleon emission ($m \to m-1$ transition), photon emission, or (what is more probable) an $m \to m+2$ transition leading to a more complicate particle–hole configuration and occurring under the effect of residual two-body interaction. After that, the same occurs once again. The new exciton state formed at the preceding step either emits a nucleon or a photon to a continuum or undergoes an $m \to m+2$ intranuclear transition, and so on. As the result of ($m \to m+2$) intranuclear transitions, the excitation energy of the composite system is distributed among an ever greater number of excitons. At the same time, $m \to m-2$ inverse transitions caused by the annihilation of one of the particle–hole pairs because of the transfer of its energy to some particle or hole are also possible. These transitions play a minor role as long as the total number of particles and holes in the system is moderately small. As their number increases, the probability of such transitions gradually grows and ultimately becomes equal to the probability of direct transitions. At this instant, the system reaches the state of thermal equilibrium either in the primary nucleus or in one of the residual nuclei, whereupon a comparatively long nucleon-evaporation process accompanied by photon emission begins. This process can be described on the basis of the evaporation model. Preequilibrium nucleon emission becomes extinct long before equilibration (as early as the first reaction stages); therefore, we will disregard inverse transitions.

Because of nucleon and photon emission, the chain of doorway-state decays ends up in the formation of some final nucleus $\{Z_{\text{fin}}, N_{\text{fin}}\}$ in the ground state. In order to trace all details of occurring processes, we will proceed as follows.

(i) We discretize the energy spectrum of excitations of the compound system with a step of $\Delta E = 0.1$ MeV and treat the resulting energy bands as discrete levels of nuclei at the energies $E_1 = E_\gamma > E_2 > \ldots > E_N = 0$.

(ii) We introduce the numbers n_π and n_ν indicating how many protons and neutrons, respectively, escaped from the $\{Z, N\}$ target nucleus before the emergence of a $\{Z', N'\} = \{Z - n_\pi, N - n_\nu\}$ intermediate nucleus (the total number of emitted nucleons is $n = n_\pi + n_\nu$).

(iii) We denote by $P(n_\pi, n_\nu, m, E_i, [T])$ and $P(n_\pi, n_\nu, E_i, [T])$ the occupation probabilities for the m-exciton states $|n_\pi, n_\nu, m, E_i, [T]\rangle$ and equilibrium states $|n_\pi, n_\nu, E_i, [T]\rangle$ in the E_i energy band of isospin T before their decay.

The isospin T is taken into account only in the decay of the giant dipole resonance; therefore, it is bracketed as an optional argument. It is also noteworthy that, in describing the decay of the giant dipole resonance, we can restrict ourselves to only two isospin values of T_0' and $T_0' + 1$ for each $\{Z', N'\}$ intermediate nucleus, where $T_0' = |(N' - Z')/2|$ is the ground-state isospin of these nucleus, since the giant dipole resonance lies at comparatively low excitation energies (not higher than 30 MeV), and this substantially simplifies the problem of taking into account isospin effects.

The decay of an arbitrary doorway state is schematically depicted in Fig. 1, where, by $|n, m\rangle$ and $|n\rangle$, we mean the m-exciton states $|n_\pi, n_\nu, m, E, [T]\rangle$ and the equilibrium states $|n_\pi, n_\nu, E, [T]\rangle$ and where $E_{\max}(n) \equiv E_{\max}(n_\pi, n_\nu) = E_\gamma - [n_\nu m_{\text{prot}} + n_\nu m_{\text{neutr}} + M(Z - n_\pi, N - n_\nu) - M(Z, N)]c^2$ is the maximum excitation energy from which the evolution of the compound system may lead to the $\{Z - n_\pi, N - n_\nu\}$ compound nucleus.

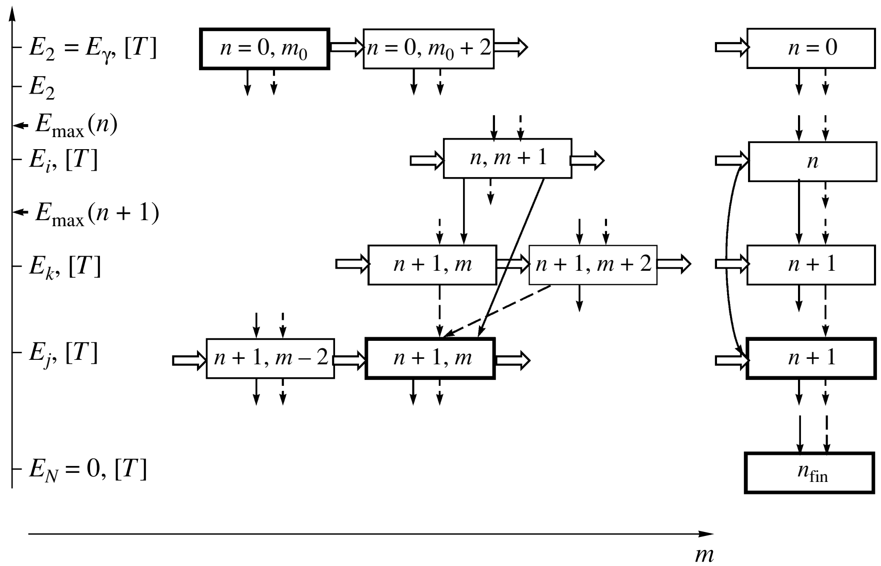

Fig. 1. Scheme of a photonucleon reaction after the formation a doorway state. The solid-line, dashed-line, and double arrows indicate, respectively, nucleon emission, photon emission, and intranuclear transitions leading to the production of yet another particle—hole pair.

The occupation probability for the m-exciton state $|n_\pi, n_\nu, m, E_i, [T]\rangle$ is equal to the sum of the probabilities for the transitions to it from states that appeared at earlier reaction states; that is,

$$P(n_\pi, n_\nu, m, E_i, [T]) = \hbar\Delta E \sum_{k=\pi,\nu} \sum_{[T']} \tag{2}$$
$$\times \sum_{E_i<E_j\le E_{\max}(n'_\pi,n'_\nu)} P(n'_\pi, n'_\nu, m+1, E_j, [T'])$$
$$\times \lambda_k(n'_\pi, n'_\nu, m+1, E_j - E_i - B'_k, E_j, [T']$$
$$\to [T])/\Gamma(n'_\pi, n'_\nu, m+1, E_j, [T']) + \hbar\Delta E$$
$$\times \sum_{[T']} \sum_{E_i<E_j\le E_{\max}(n_\pi,n_\nu)} P(n_\pi, n_\nu, m, E_j, [T'])$$
$$\times \lambda_\gamma^{(1)}(n_\pi, n_\nu, m, E_j - E_i, E_j, [T']$$
$$\to [T])/\Gamma(n_\pi, n_\nu, m, E_j, [T']) + \hbar\Delta E$$
$$\times \sum_{[T']} \sum_{E_i<E_j\le E_{\max}(n_\pi,n_\nu)} P(n_\pi, n_\nu, m$$
$$+ 1, E_j, [T'])\lambda_\gamma^{(2)}(n_\pi, n_\nu, m+1, E_j$$
$$- E_i, E_j, [T'] \to [T])/\Gamma(n_\pi, n_\nu, m+1, E_j, [T'])$$
$$+ P(n_\pi, n_\nu, m-2, E_i, [T])$$
$$\times \Gamma^{\downarrow}(n_\pi, n_\nu, m-2, E_i, [T])/\Gamma(n_\pi, n_\nu,$$
$$m-2, E_i, [T]),$$

where $n'_\pi = n_\pi - \delta_{k\pi}$; $n'_\nu = n_\nu - \delta_{k\nu}$; B'_k is the separation energy for a nucleon of type k (a proton or a neutron) from the $\{Z - n'_\pi, N - n'_\nu\}$ nucleus; $\lambda_k(n'_\pi, n'_\nu, m+1, \varepsilon, E, [T'] \to [T])$ is the rate of the $(T' \to T)$ decay of the state $|n'_\pi, n'_\nu, m+1, E, [T']\rangle$ with the emission of a k-type nucleon of energy ε to a continuum; $\Gamma(n_\pi, n_\nu, m, E, [T])$ is the total width of the state $|n_\pi, n_\nu, m, E, [T]\rangle$; $\Gamma^{\downarrow}(n_\pi, n_\nu, m, E, [T])$ is that component of this width which is due to intranuclear transitions; and $\lambda_\gamma^{(1)}(n_\pi, n_\nu, m, \varepsilon, E, [T'] \to [T])$ and $\lambda_\gamma^{(2)}(n_\pi, n_\nu, m, \varepsilon, E, [T'] \to [T])$ are the components of the rate of m-exciton state decay occurring via photon emission, respectively, without and with a change in the number of excitons $[\lambda_\gamma(\ldots) = \lambda_\gamma^{(1)}(\ldots) + \lambda_\gamma^{(2)}(\ldots)$ is the total rate of decay of this state via photon emission] [37].

An expression for the population of the equilibrium state $|n_\pi, n_\nu, E_i, [T]\rangle$ can be obtained in a similar way. Specifically, we have

$$P(n_\pi, n_\nu, E_i, [T]) = P(n_\pi, n_\nu, m_{\text{mean}}, E_i, [T]) \tag{3}$$
$$+ \hbar\Delta E \sum_{k=\pi,\nu} \sum_{[T']}$$
$$\times \sum_{E_i<E_j\le E_{\max}(n'_\pi,n'_\nu)} P(n'_\pi, n'_\nu, E_j, [T'])$$
$$\times \lambda_j(n'_\pi, n'_\nu, E_j - E_i - B'_k, E_j, [T']$$
$$\to [T])/\Gamma(n'_\pi, n'_\nu, E_j, [T'])$$
$$+ \hbar\Delta E \sum_{[T']} \sum_{E_i<E_j\le E_{\text{макс}}(n_\pi,n_\nu)} P(n_\pi, n_\nu, E_j, [T'])$$
$$\times \lambda_\gamma(n_\pi, n_\nu, E_j - E_i, E_j, [T']$$
$$\to [T])/\Gamma(n_\pi, n_\nu, E_j, [T']),$$

where we apply the same notation as in Eq. (2) bur to equilibrium states; also, $m_{\mathrm{mean}} = 0.8(aE_i)^{1/2}$ is the mean number of excitons in the equilibrium state (a is the level-density parameter).

The recursion relations (2) and (3) make it possible to calculate the whole chain of occupation probabilities for exciton and equilibrium states of the compound system since $P(n_\pi = 0, n_\nu = 0, m = m_0, E_\gamma, [T]) = 1$ and $P(n_\pi = 0, n_\nu = 0, E_\gamma, [T]) = P(n_\pi = 0, n_\nu = 0, m = m_{\mathrm{mean}}, E_\gamma, [T])$.

Knowing all of these probabilities, one can readily calculate the total exclusive photonucleon cross sections corresponding to the emission of specific numbers of protons and neutrons from the target nucleus and the total photonucleon spectra integrated with respect to the emission angle.

For example, the exclusive photonucleon cross section $\sigma(n_\pi, n_\nu, E_\gamma)$ is obviously given by the expression

$$\sigma(n_\pi, n_\nu, E_\gamma) = \sum_s \sigma_s(E_\gamma) P_s(n_\pi, n_\nu, E = 0, [T_{\mathrm{fin}}]), \tag{4}$$

where summation is performed over all photonucleon-cross-section components [see expression (1)] to each of which its own doorway state $|s\rangle$ corresponds and $T_{\mathrm{fin}} = |(N - Z - n_\nu + n_\pi)/2|$ is the ground-state isospin of the final nucleus.

The total photoproton and photoneutron energy spectra integrated with respect to the emission angle can be calculated by the formula

$$\frac{d\sigma_k(\varepsilon, E_\gamma)}{d\varepsilon} = \hbar \sum_s \sigma_s(E_\gamma) \tag{5}$$
$$\times \sum_{n_\pi} \sum_{n_\nu} \sum_{[T]} \sum_{[T']} \sum_{B_k < E_j \le E_{\max}(n_\pi, n_\nu)} \Bigg\{ P_s(n_\pi, n_\nu, E_j, [T]) \lambda_k^{(s)}(n_\pi, n_\nu, \varepsilon, E_j, [T] \to [T'])/\Gamma^{(s)}(n_\pi, n_\nu, E_j, [T]) + \sum_{m=m_0}^{m_{\mathrm{mean}}-1} P_s(n_\pi, n_\nu, m, E_j, [T]) \times \lambda_k^{(s)}(n_\pi, n_\nu, m, \varepsilon, E_j, [T] \to [T']) \times [\Gamma^{(s)}(n_\pi, n_\nu, m, E_j, [T])]^{-1} \Bigg\},$$

where $k = \pi$ and $k = \nu$ for protons and neutrons, respectively.

4. ISOSPIN EFFECTS

We have already indicated in the Introduction that, in considering photonucleon reactions in the energy range of $E_\gamma \lesssim 30$ MeV dominated by dipole photoabsorption followed by the excitation of the giant dipole resonance, it is important to take into account isospin effects. In estimating the decay features $\lambda_k(m, \varepsilon, E)$ and $\lambda_k(\varepsilon, E), \ldots (k = \pi, \nu)$ of exciton and equilibrium states on the basis of semiclassical statistical models [8–14], these effects are disregarded, which leads to a catastrophic underestimation of the photoproton yield in medium-mass and heavy nuclei.

Meanwhile, it is not difficult to take these effects into account in calculating such features. In order to avoid the repetition of the same arguments, we combine the formulas that describe the emission of preequilibrium and equilibrium photonucleons, bracketing the number of excitons, whereby we imply that we take into account this argument only at the preequilibrium reaction stage.

We will now estimate the probability for the transition per unit time from the state $|[m], E, T\rangle$, $T = T_0, T_0 + 1$ to the state $|[m-1], E', T'\rangle$, $T' = T_0', T_0' + 1$ (where T_0 and T_0' are the ground-state isospins of, respectively, the initial and the final nucleus) with the emission a nucleon belonging to the $k = \pi, \nu$ type (a proton or a neutron) and having an energy $\varepsilon \pm d\varepsilon/2$ to a continuum ($E' = E - B_k - \varepsilon$, B_k being the separation energy for a nucleon of type k).

We denote by A the group of states $|[m], E, T\rangle$ concentrated in the energy range $E \pm \Delta E/2$ and by B the group of compound-system states that includes the states $|[m-1], E', T'\rangle$ of the final nucleus in the energy range $E' \pm \Delta E/2$ plus the free-nucleon states at the energy $\varepsilon \pm d\varepsilon/2$. According to the detailed-balance principle, the probabilities $P_k(A \to B)$ and $P_k(B \to A)$ for the transitions from A to group B and from group B to group A, respectively, then satisfy the relation

$$\frac{P_k(A \to B)}{\mathrm{g}_B} = \frac{P_k(B \to A)}{\mathrm{g}_A}, \tag{6}$$

where $\mathrm{g}_A = \omega([m], E, T)\Delta E$ is the statistical weight of states of group A; $\mathrm{g}_B = \omega([m-1], E', T')\rho_{\mathrm{fr}}(\varepsilon) \times \Delta E d\varepsilon$ is the statistical weight of states of group B; $\omega([m], E, T)$ and $\omega([m-1], E', T')$ are the densities of states in, respectively, the initial and the final nucleus at the respective energies; and

$$\rho_{\mathrm{fr}}(\varepsilon) = \frac{V(2s+1)}{2\pi^2\hbar^3}\sqrt{2\mu^3\varepsilon} \tag{7}$$

is the density of states for a free nucleon lying in the volume V (here, $s = 1/2$ is the spin of the nucleon and μ is its reduced mass).

The probability for the inverse transition $B \to A$ can be represented as the product of three factors; that is,

$$P_k(B \to A) = V^{-1}\sqrt{\frac{2\varepsilon}{\mu}}\sigma_k^{\mathrm{inv}}(\varepsilon) \tag{8}$$
$$\times \frac{\omega([m], E, T)}{\omega([m], E)} \times f_{B,A}(T' \to T).$$

Here, the first factor determines the probability for the inverse process (nucleon capture by the final nucleus) in the case where the states does not differ in isospin either in the initial or in the final nucleus. The inverse-reaction cross section

$$\sigma_k^{\mathrm{inv}}(\varepsilon) = \frac{1}{2}\pi\lambda\!\!\!^{-2}\sum_{jl}(2j+1)T_{jl}^k(\varepsilon),$$

where $T_{jl}^k(\varepsilon)$ is the transmission coefficient for a nucleon belonging to type k and having an orbital angular momentum l and a total angular momentum j, can be calculated on the basis of the optical model. The second factor takes into account the circumstance that, in the initial nucleus, we are interested in the population of only those states that have a fixed isospin, $T = T_0$ or $T_0 + 1$ ($\omega([m], E) = \omega([m], E, T_0) + \omega([m], E, T_0 + 1)$ is the total density of states in the initial nucleus at the energy E). The last, third, factor characterizes the fraction of states $|[m], E, T\rangle$ populated upon the $T' \to T$ transitions. Since the probability of this event is proportional to the product of the density of states $|[m-1], E', T'\rangle$ and the square of the respective Clebsch–Gordan coefficient, the factor $f_{B,A}(T' \to T)$ can obviously be represented in the form

$$f_{B,A}(T' \to T) = \omega([m-1], E', T') \tag{9}$$
$$\times \left(T'T_{0z} - t_{zk}\frac{1}{2}t_{zk}\middle|TT_{0z}\right)^2$$
$$\times \left(\omega([m-1], E', T_0')\left(T_0'T_{0z}\right.\right.$$
$$\left.- t_{zk}\frac{1}{2}t_{zk}\middle|TT_{0z}\right)^2 + \omega([m-1], E', T_0'+1)$$
$$\left.\times \left(T_0'+1T_{0z} - t_{zk}\frac{1}{2}t_{zk}\middle|TT_{0z}\right)^2\right)^{-1},$$

where $T_{0z} = (N - Z)/2$ is the z projection of the initial-nucleus isospin and t_{zk} is the z projection of the emitted-nucleon isospin.

From Eqs. (6)–(8), it follows that the rate of decay of the initial-nucleus state $|[m], E, T\rangle$ to the final-nucleus state $|[m-1], E', T'\rangle$ via the emission of a k-type nucleon with energy ε is

$$\lambda_k([m], \varepsilon, E, T \to T') \tag{10}$$
$$= P_k(A \to B)/d\varepsilon = \frac{2s+1}{\pi^2\hbar^3}\mu\varepsilon\sigma_k^{\mathrm{inv}}(\varepsilon)$$
$$\times \frac{\omega([m-1], E', T')}{\omega([m], E)} f_{B,A}(T' \to T),$$

where the factor $f_{B,A}(T' \to T)$ is given be expression (9).

In medium-mass and heavy nuclei, $\omega([m-1], E', T_0') \approx \omega([m-1], E') \gg \omega([m-1], E', T_0'+1)$ and $f_{B,A}(T_0' \to T_0) \approx 1$ in the energy region being considered; therefore, we can disregard transitions to $T' = T_0' + 1$ final-nucleus states in describing the decay features of the $T_<$ giant-dipole-resonance component. Formula (10) then transforms into the standard formula of the statistical model [19]. In the decay of the $T_>$ giant-dipole-resonance component via proton emission, the situation is similar, since this decay proceeds predominantly to the T_0' states of the final nucleus. In the decay of the $T_>$ giant-dipole-resonance component via neutron emission, only the $(T_0' + 1)$ states of the final state are available (concurrently, we have $f_{B,A}(T_0' + 1 \to T_0 + 1) = 1$). The rate of this decay is proportional to $\omega([m-1], E', T_0' + 1)$ and is substantially lower than the rate of decay via proton emission, $\lambda_\pi([m], \varepsilon, E, T_0 + 1 \to T_0') \propto \omega([m-1], E', T_0')$, and this explains a predominant proton emission in the $T_>$ reaction channel for medium-mass and heavy nuclei.

The densities of final states in massive nuclei can be approximated by the expressions

$$\omega([m-1], E', T_0') \approx \omega([m-1], E'), \tag{11}$$
$$\omega([m-1], E', T_0'+1) \tag{12}$$
$$\approx \begin{cases} \omega([m-1], E' - \Delta_1') & \text{for } E' \geq \Delta_1', \\ 0 & \text{for } E' < \Delta_1', \end{cases}$$

where Δ_1' is the energy of the first excited level with isospin $T_0' + 1$ in the final nucleus.

In lighter nuclei ($A < 50$ MeV), it is necessary to take into account both branches of T transitions described by expressions (10). It is also necessary to refine the estimates of the densities of final states characterized by various values of the isospin quantum number. We represent these densities of states in the form

$$\omega([m-1], E', T_0') \tag{13}$$
$$\approx \omega([m-1], E')\frac{1}{1+q(E')},$$
$$\omega([m-1], E', T_0'+1) \tag{14}$$
$$\approx \omega([m-1], E')\frac{q(E')}{1+q(E')},$$

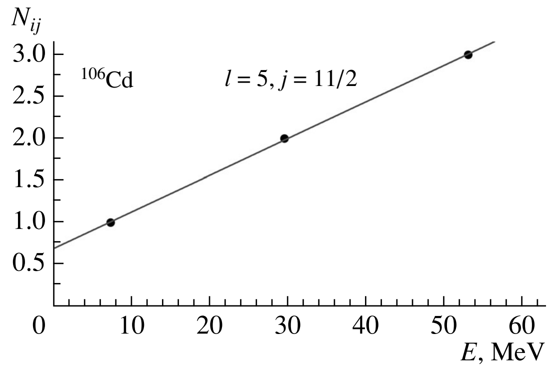

Fig. 2. Change in the number of ljm levels in the ^{106}Cd (closed circles) as the excitation energy grows.

where

$$q(E') \approx \begin{cases} \omega([m-1], E'-\Delta_1')/\omega([m-1], E') \\ \text{for } \; E' \geq \Delta_1', \\ 0 \quad \text{for } \; E' < \Delta_1'. \end{cases} \tag{15}$$

For $q(E') \to 0$, the estimates in (13) and (14) go over to the estimates in (11) and (12). Moreover, they satisfy the relation $\omega([m-1], E') = \omega([m-1], E', T_0') + \omega([m-1], E', T_0'+1)$.

5. PHOTON DECAY CHANNEL

In describing the photon decay channel, we can retain ordinary formulas of statistical models, since, in the energy region where the inclusion of the isospin is of importance, photon emission is due primarily to decay to final-nucleus levels of isospin T_0' (equal to the ground-state isospin), their density being substantially higher then the density of states with isospin $T_0'+1$.

However, there is a distinction between the features of decays via nucleon emission and the features of decays via photon emission. The former are averaged over a large number of possible values of the angular momentum J, but, for the latter, selection rules in J and in parity must be taken into account since the photon channel is dominated by $E1$-emission processes associated with the excitation of the giant dipole resonance. This can be done with the aid of a special factor introduced in the rate of the decay of preequilibrium and equilibrium states via photon emission.

For example, the rate of the equilibrium gamma transition having an energy ε_γ and going from some state of the intermediate nucleus at an excitation energy E to the final-nucleus state at the energy $E' = E - \varepsilon_\gamma$ can be represented in the form

$$\lambda_\gamma(\varepsilon_\gamma, E) = \frac{\varepsilon_\gamma^2}{\pi^2 \hbar^3 c^2} \sigma_{\text{dip}}(\varepsilon_\gamma) c_{J\pi}(E, E') \frac{\omega_f(E')}{\omega_i(E)}, \tag{16}$$

where $\sigma_{\text{dip}}(\varepsilon_\gamma)$ is the cross section for $E1$ photoabsorption [38]; $\omega_i(E)$ and $\omega_f(E')$ are the total densities of equilibrium states in, respectively, the initial and the final nucleus; and the $c_{J\pi}(E, E')$ is a correcting factor that permits taking into account the effect of selection rules in the angular momentum and parity on the $E1$-transition probability.

As follows from [39], the dependence of the density of nuclear states on the angular momentum J and parity $\pi = \pm 1$ has the form

$$\omega(E, J, \pi) = F_\pi(\pi) F_J(J, E) \omega(E), \tag{17}$$

where

$$F_\pi(\pi) = \frac{1}{2}, \tag{18}$$

$$F_J(J, E) = \frac{2J+1}{2\sigma^2(E)} \times \exp\left[-\left(J+\frac{1}{2}\right)^2 \Big/ (2\sigma^2(E))\right] \tag{19}$$

($\sigma^2(E) = 0.0888 A^{2/3} \sqrt{aE}$ and a is the level-density parameter [39]).

From Eqs. (17)–(19), it follows that the factor $c_{J\pi}(E, E')$ can be approximated by the expression

$$c_{J\pi}(E, E') \approx F_\pi(\pi) \left[\sum_{j=0}^{1} \int_0^\infty F_J(J, E) F_J(J+j, E') dJ + \int_1^\infty F_J(J, E) F_J(J-1, E') dJ \right]. \tag{20}$$

6. INFLUENCE OF THE DOORWAY-STATE STRUCTURE ON THE SEMIDIRECT PHOTOEFFECT

In the shell model, the doorway-dipole state of an axisymmetric nucleus is treated as a coherent superposition of $1p1h$ states, $|\alpha, \beta^{-1}\rangle$, where

$$|\alpha\rangle = \sum_{lj \in \alpha} c_{lj} |nljm\rangle$$

and $|\beta\rangle$ stands for single-particle states having a specific value of the projection m of the angular momentum onto the symmetry axis of the nucleus and corresponding, for example, to the Nilsson potential ($|nljm\rangle$ are eigenstates of a spherical harmonic oscillator).

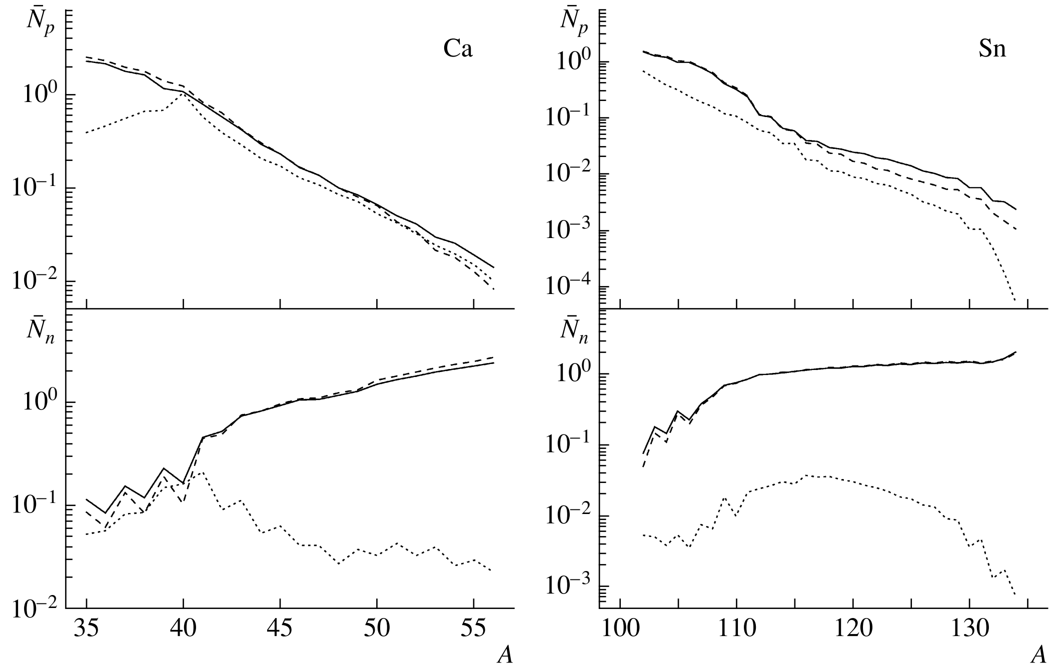

Fig. 3. Mean numbers of protons, $\bar{N}_p$ and neutrons, $\bar{N}_n$, emitted into the energy range of $E_\gamma = 0$–30 MeV versus the mass number A for calcium and tin isotopes. The solid and dashed curves stand for the results of the calculations performed, respectively, with and without allowance for the structure of the doorway dipole state. The dotted curves represent the contribution of the decay of the $T_>$ component of the giant dipole resonance for the calculation that takes into account the structure of the doorway state.

For the doorway dipole state at an energy E, the rate of decay accompanied by the emission of a nucleon with energy ε from the nucleus can be represented in the form

$$\lambda_{\rm dip}(\varepsilon, E) \quad (21)$$
$$= \sum_{\alpha\beta^{-1}} P_{\alpha\beta^{-1}} \sum_{lj\in\alpha} c_{lj}^2 \lambda(\alpha\beta^{-1}, E; \varepsilon ljm),$$

where $P_{\alpha\beta^{-1}}$ is the relative probability for the dipole excitation of the configuration $|\alpha\beta^{-1}\rangle$ [it is proportional to the squared matrix element of the single-particle $E1$ transition, $\langle\alpha|2t_z r Y_{1M}(\hat{\mathbf{r}})|\beta\rangle^2$; the sum of such probabilities for all nucleon transitions of the same type must be equal to unity],

$$\lambda(\alpha\beta^{-1}, E; \varepsilon ljm) \quad (22)$$
$$= \frac{2s+1}{\pi^2\hbar^3}\mu\varepsilon\sigma_{ljm}^{\rm inv}(\varepsilon)\frac{\omega(\beta^{-1}, E')}{\omega(\beta^{-1}, ljm; E)}$$

is the probability for the decay per unit time of the configuration $|\alpha\beta^{-1}, E\rangle$ with the emission of a εljm nucleon, $\sigma_{ljm}^{\rm inv}(\varepsilon) = \frac{1}{2}\pi\lambda\!\!\!^{-2} T_{jl}(\varepsilon)$ is the cross section for the absorption of a εljm nucleon, $\omega(\beta^{-1}, E')$ is the distribution density for a hole β^{-1} in the vicinity of the energy $\varepsilon_{\beta^{-1}}$ ($E' = E - B_{\rm thr} - \varepsilon$),

$$\omega(\beta^{-1}, ljm; E) \quad (23)$$
$$= \int\limits_0^{E-B_{\rm thr}} \omega_{ljm}(\varepsilon)\omega(\beta^{-1}, E - B_{\rm thr} - \varepsilon)d\varepsilon$$

is the total density of the configurations $|\beta^{-1}, ljm\rangle$ at the energy E that have preset quantum numbers $\{\beta ljm\}$, and $\omega_{ljm}(\varepsilon)$ is the total density of ljm states to which a nucleon of energy ε can be captured.

Figure 2 shows a typical picture of how, in the Nilsson spherical potential, the number of single-particle levels that have fixed quantum numbers ljm changes as the particle excitation energy grows. From this figure, one can see that the number of such states grows with energy linearly: $N_{lj} = a_{lj} + {\rm g}_{lj}\varepsilon$. Therefore, the single-particle level densities $\omega_{ljm}(\varepsilon) = d[N_{lj}(\varepsilon)]/d\varepsilon$ can be approximated by the constants ${\rm g}_{lj}$ found in this way. The hole-distribution density $\omega(\beta^{-1}, E')$ appearing in expressions (22) and (23) can be approximated by a Breit–Wigner curve normalized to unity in the range of $0 \le E' \le \infty$, its width being estimated on the basis of the optical model.

In [34], the $T_<$ and $T_>$ components of the giant dipole resonance were separated within the semimicroscopic model of vibrations that was proposed in [10, 33]. If the spread of the energies of single-particle transitions and pair correlations in the $|T_0, T_{0z}\rangle$ ground state of the nucleus are disregarded,

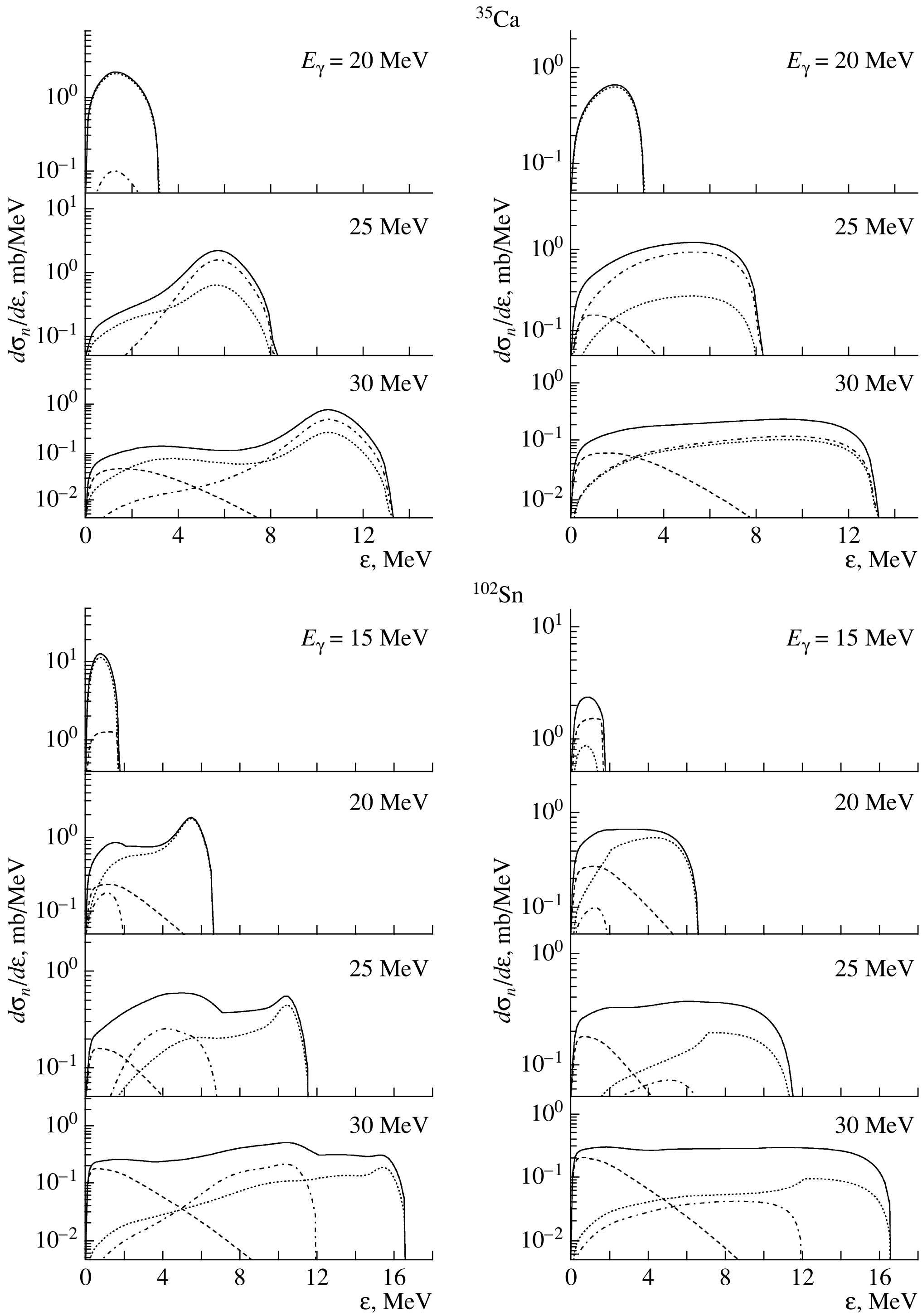

Fig. 4. Photoneutron spectra for the ^{35}Ca and ^{102}Sn nuclei, which lie near the lower mass boundary of the isotopic chains, according to calculations performed, respectively, with (left-hand panels) and without (right-hand panels) allowance for the structure of the doorway state. Here, E_γ is the gamma-irradiation energy, while ε is the emitted-nucleon energy. The solid curves represent the total spectrum. The dashed curves correspond to the evaporation section of the spectrum. The dotted curves stand for the contribution to the spectrum from the first preequilibrium nucleon emitted by the $T_<$ component of the giant dipole resonance. The dash-dotted curves represent the contribution of the first prequilibrium nucleon emitted by the $T_>$ component of the giant dipole resonance.

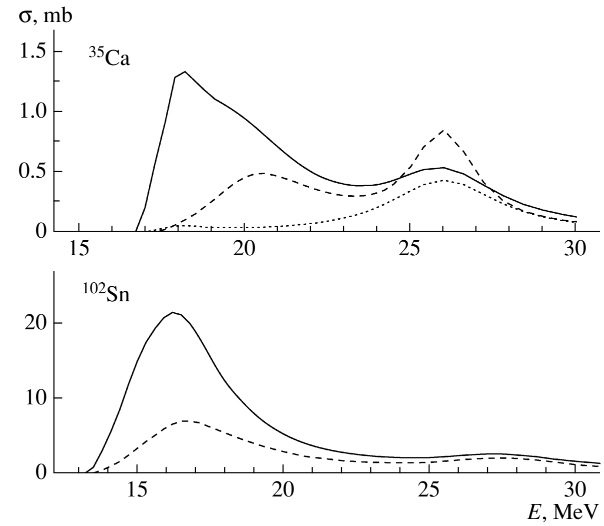

Fig. 5. Cross section for the (γ, n) reactions on the highly neutron-deficient nuclei ^{35}Ca and ^{102}Sn. The solid and dashed curves stand for the results of the calculations performed, respectively, with and without allowance for the structure of the doorway state. The dotted curves represent the contribution of the $T_>$ component of the giant dipole resonance for the calculation that takes into account the structure of the doorway state.

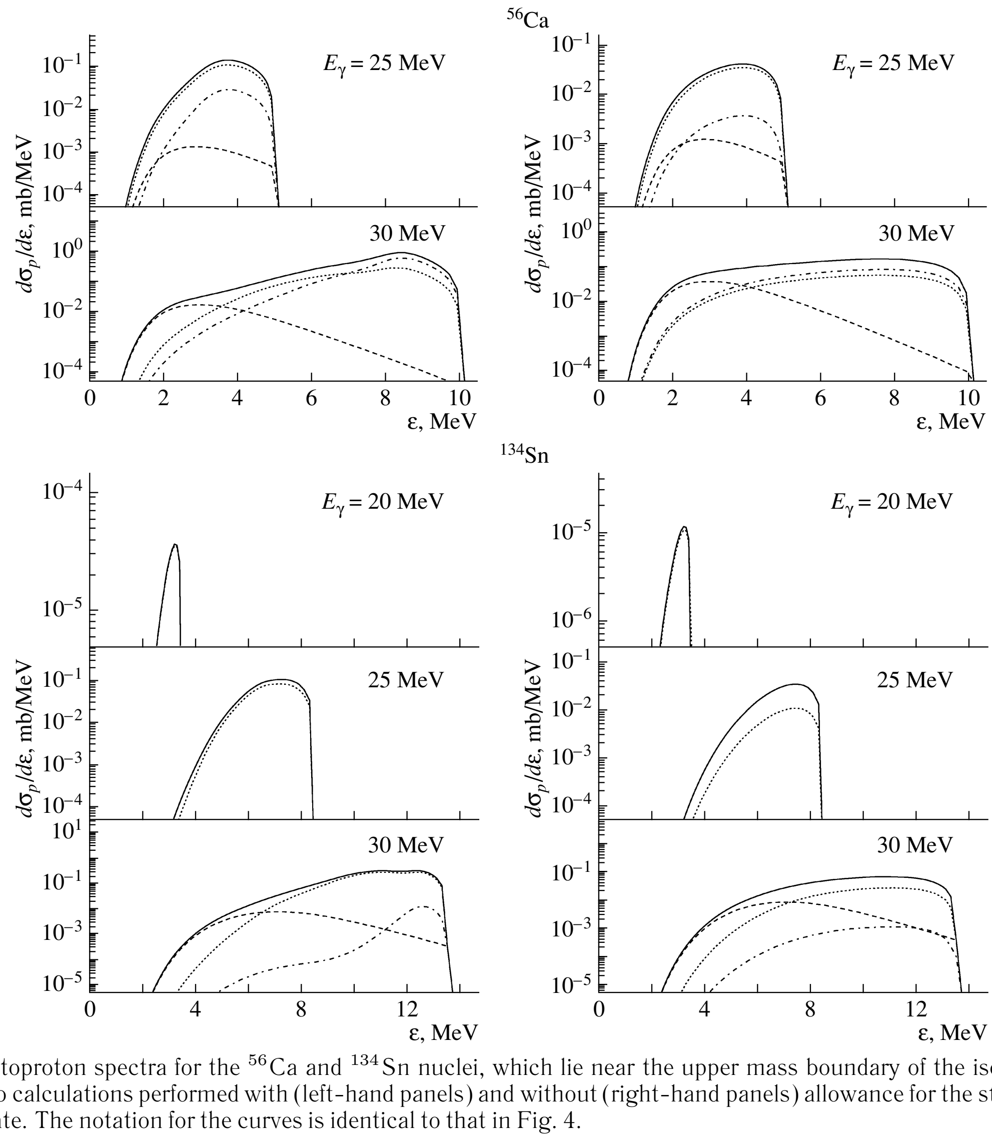

Fig. 6. Photoproton spectra for the ^{56}Ca and ^{134}Sn nuclei, which lie near the upper mass boundary of the isotopic chains, according to calculations performed with (left-hand panels) and without (right-hand panels) allowance for the structure of the doorway state. The notation for the curves is identical to that in Fig. 4.

then the wave functions for the $T_<$ and $T_>$ dipole states can approximately be represented in the form

$$|\Psi_{1M}(T_0+1, T_{0z})\rangle = C_> \quad (24)$$
$$\times \sum_{\alpha\in\{\alpha_n\}} \sum_{\beta\in\{\beta_p\}} \langle\alpha|2t_z r Y_{1M}(\hat{\mathbf{r}})|\beta\rangle a_\alpha^+ a_\beta |T_0, T_{0z}\rangle,$$
$$|\Psi_{1M}(T_0, T_{0z})\rangle = C_< \quad (25)$$
$$\times \left[\sum_\alpha \sum_\beta \langle\alpha|2t_z r Y_{1M}(\hat{\mathbf{r}})|\beta\rangle a_\alpha^+ a_\beta - \frac{1}{T_0+1}\right.$$
$$\left.\times \sum_{\alpha\in\{\alpha_n\}} \sum_{\beta\in\{\beta_p\}} \langle\alpha|2t_z r Y_{1M}(\hat{\mathbf{r}})|\beta\rangle a_\alpha^+ a_\beta |T_0, T_{0z}\rangle\right],$$

where summation $\sum_{\alpha\in\{\alpha_n\}}\sum_{\beta\in\{\beta_p\}}$ is performed only over single-particle neutron and proton transitions that proceed between levels occupied in protons and levels vacant for neutrons and where $C_>$ and $C_<$ are normalization constants.

Relations (24) and (25) make it possible to estimate the decay features of doorway states for the $T_<$ and $T_>$ components of the giant dipole resonance individually. These relations were obtained under the assumption that the target nucleus is neutron-rich. If this is not so, it is necessary to make the substitutions $\{\alpha_n\} \to \{\alpha_p\}$ and $\{\beta_p\} \to \{\beta_n\}$ in them.

7. APPLICATION OF THE MODEL TO DESCRIBING PHOTONUCLEON REACTIONS ON CALCIUM AND TIN ISOTOPES FOR $E_\gamma \lesssim 30$ MeV

The corrections introduced in the model make it possible to found out how, in the energy region of $E_\gamma \lesssim 30$ MeV, special features of photonucleon reactions change upon going over from proton-rich to neutron-rich isotopes of moderately light and medium-mass nuclei. As objects of this investigation, we choose calcium and tin isotopes: $^{35-56}$Ca and $^{102-134}$Sn.

7.1. Dependence of Proton and Neutron Yields on the Isotope Mass Number

Figure 3 shows how the results of the calculations in the energy range of $E_\gamma = 0{-}30$ MeV for the mean numbers of protons and neutrons emitted in the reaction change in response to changes in the mass numbers of calcium and tin isotopes:

$$\bar{N}_p = \sum_{n_\pi=1}^{\infty}\sum_{n_\nu=0}^{\infty}\int_0^{30} n_\pi \sigma(n_\pi, n_\nu, E_\gamma) \quad (26)$$
$$\times dE_\gamma \left[\sum_{n_\pi=1}^{\infty}\sum_{n_\nu=0}^{\infty}\int_0^{30} \sigma(n_\pi, n_\nu, E_\gamma) dE_\gamma\right]^{-1},$$
$$\bar{N}_n = \sum_{n_\pi=0}^{\infty}\sum_{n_\nu=1}^{\infty}\int_0^{30} n_\nu \sigma(n_\pi, n_\nu, E_\gamma) \quad (27)$$
$$\times dE_\gamma \left[\sum_{n_\pi=0}^{\infty}\sum_{n_\nu=1}^{\infty}\int_0^{30} \sigma(n_\pi, n_\nu, E_\gamma) dE_\gamma\right]^{-1}.$$

From this figure, it can be seen that, despite the suppressing effect of the Coulomb barrier, the photodisintegration of isotopes characterized by a high neutron deficit is dominated by the proton decay channel owing to the smallness of the proton thresholds. On the other hand, the thresholds for neutron separation are low in nuclei featuring a large excess of neutrons, so that the mean number of neutrons emitted per reaction event grows sharply.

The solid and dashed curves in Fig. 3 represent the results of the calculations performed, respectively, with and without allowance for the structure of the doorway dipole state. Comparing these curves, we can conclude that a more detailed description of the semidirect photoeffect becomes important near the lower and upper mass boundaries of the isotopic chains. Standard statistical models obviously underestimate the role of semidirect reactions. The result of this is that, in the boundary regions, where the proton and neutron thresholds are sharply different, the yield of nucleons for which the separation threshold is high (neutrons for small values of A and protons for its large values) proves to be underestimated. The fact that the chances for their emission decrease substantially at the evaporation stage because of photon emission also contributes to this. Figure 3 indicates that the semidirect effect should make a substantial contribution to the total yield of photonucleons in proton- and neutron-rich nuclei.

The dotted curves in Fig. 3 stand for the contribution of processes associated with the decay of the $T_>$ giant-dipole-resonance component. From Fig. 3, one can see that two regions stand out for calcium isotopes: the region of $A < 40$, where $N < Z$, and the region of $A > 40$, where $N > Z$. The giant-dipole-resonance component in question decays predominantly through the neutron channel in the first of these regions and through the proton channel in the second one. In the case of tin isotopes, the $T_>$ component of the giant dipole resonance decays predominantly through the proton channel, making a significant contribution to the total proton yield. This is indicative of the importance of taking into account isospin effects in describing photonucleon reactions.

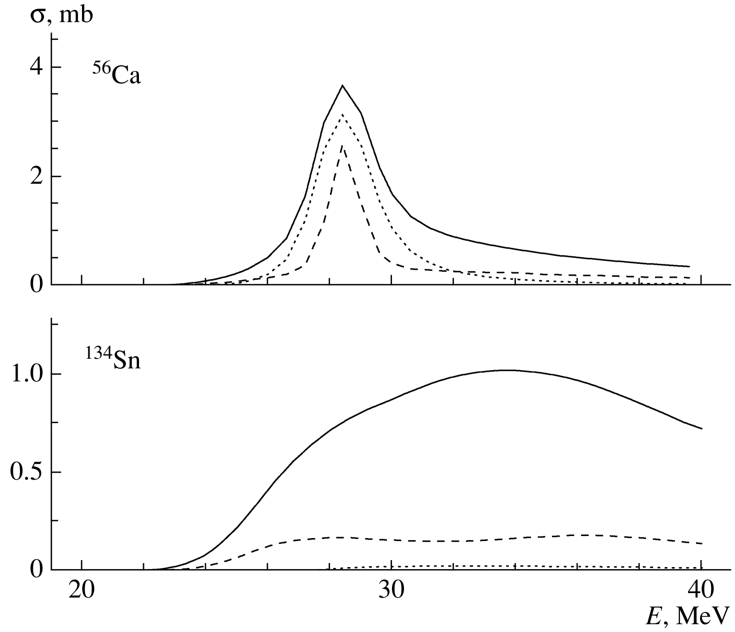

Fig. 7. Cross section for the (γ, p) reactions on the highly proton-deficient nuclei ^{56}Ca и ^{134}Sn. The notation for the curves is identical to that in Fig. 5.

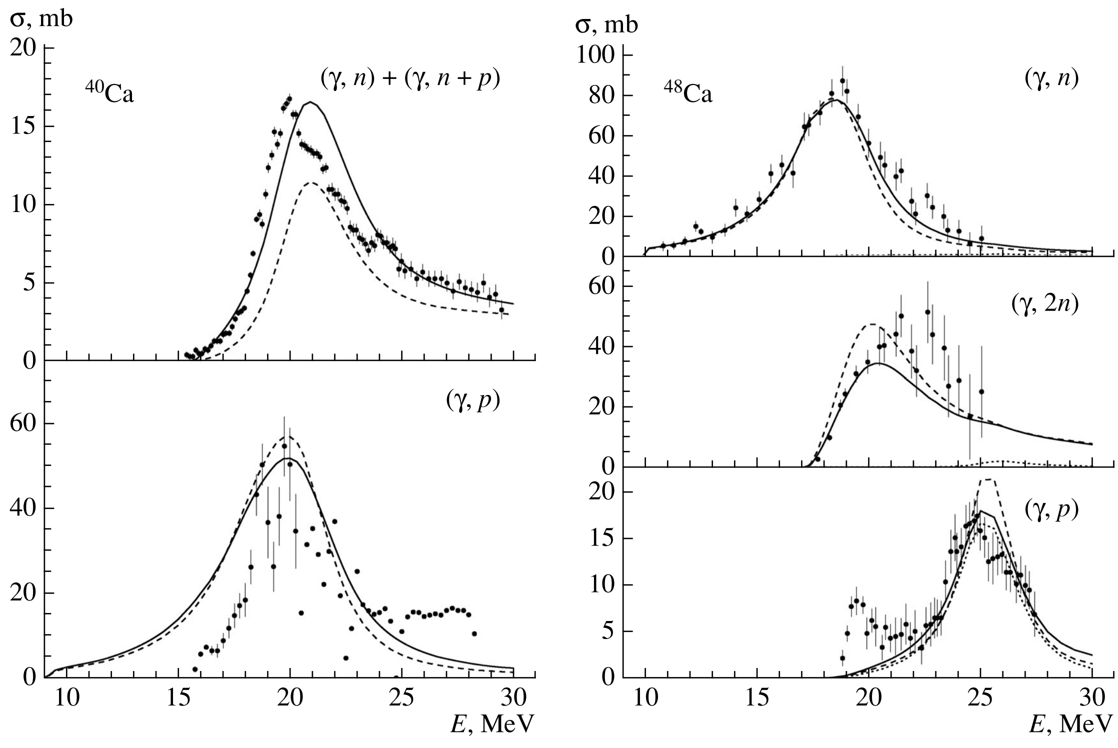

Fig. 8. Cross sections for the photonucleon reactions on ^{40}Ca and ^{48}Ca nuclei. The displayed experimental data (points with error bars) were taken from [41, 42] for ^{40}Ca and from [43] for ^{48}Ca. The notation for the curves is identical to that in Fig. 5.

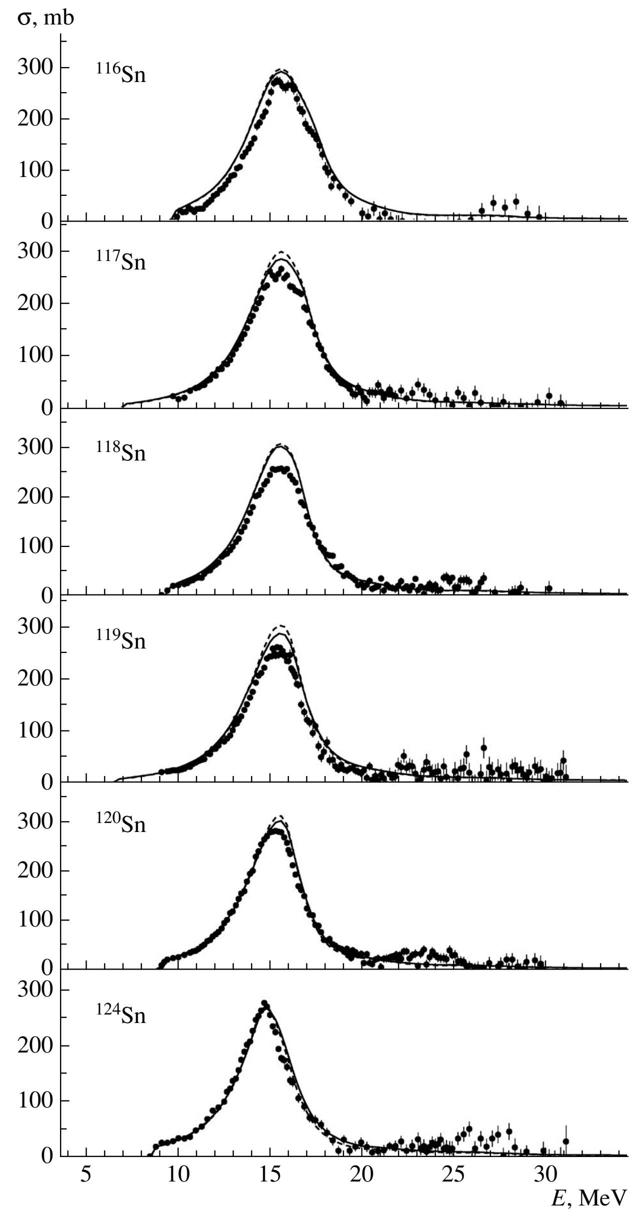

Fig. 9. Cross sections for the $(\gamma, n) + (\gamma, n + p)$ reactions on the tin isotopes $^{116-120,124}$Sn in the region around the giant dipole resonance. The displayed experimental data were borrowed from [44]. The notation for the curves is identical to that in Fig. 5.

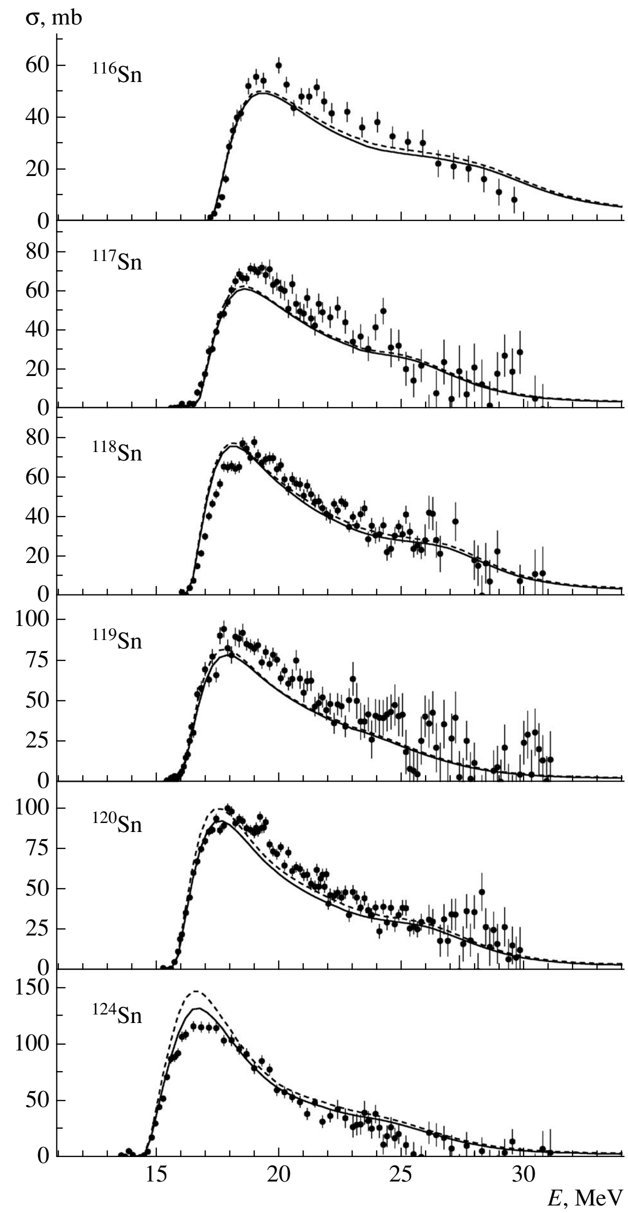

Fig. 10. Cross sections for the $(\gamma, 2n) + (\gamma, 2n + p)$ reactions on the tin isotopes $^{116-120,124}$Sn in the region around the giant dipole resonance. The displayed experimental data were borrowed from [44]. The notation for the curves is identical to that in Fig. 5.

A steep descent of the curve representing the yield of protons from the $T_>$ component of the giant dipole resonance in the ^{132}Sn region is due to a sharp decrease in the respective component: by way of example, we indicate that, according to the estimation of Goulard and Fallieros [40], the ratio of the dipole strengths for the $T_>$ and $T_<$ components is as small as 0.001 for ^{134}Sn. We also highlight a sawtooth character of the curves in Fig. 3. The observed breaks on the curves are due to the jumplike increase in the neutron yield (because of a decrease in the neutron threshold) upon going over from an odd–odd to the neighboring even–odd isotope.

7.2. Neutron Photoeffect near the Lower Mass boundary of the Isotopic Chain and Proton Photoeffect near Its Upper Mass Boundary

Figure 4 shows photoneutron spectra calculated for the highly neutron-deficient nuclei ^{35}Ca and ^{102}Sn

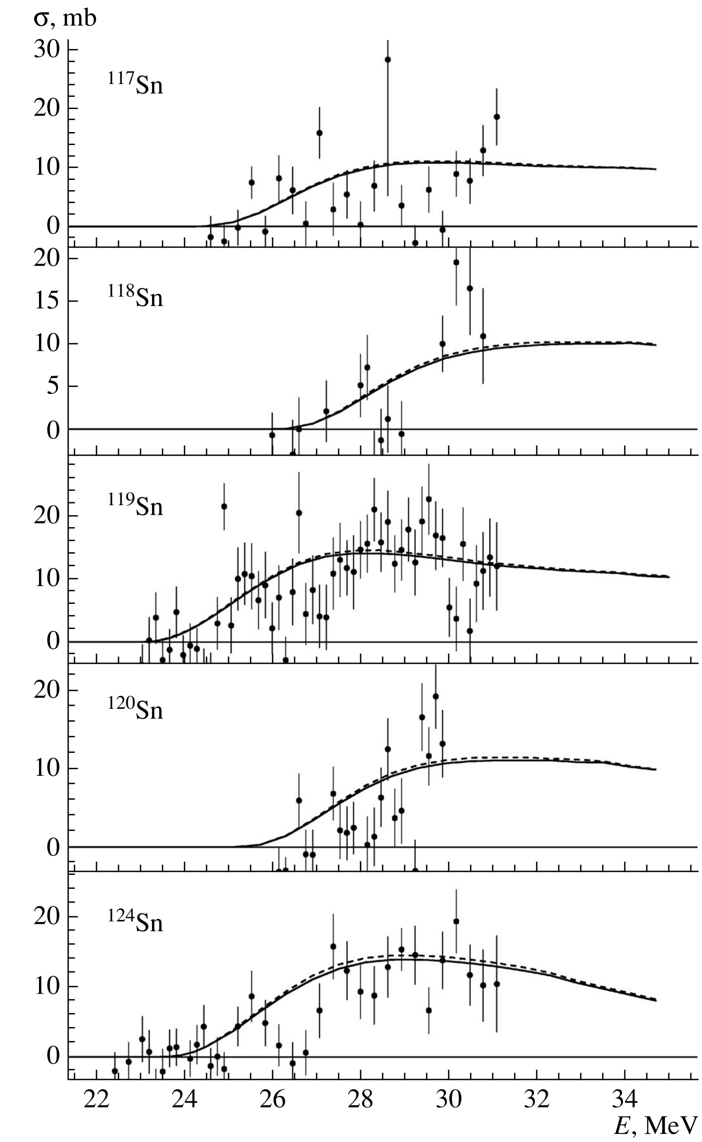

Fig. 11. Cross sections for the $(\gamma, 3n)$ reactions on the tin isotopes $^{117-120,124}$Sn in the region in the region around the giant dipole resonance. The displayed experimental data were borrowed from [44]. The notation for the curves is identical to that in Fig. 5.

with and without allowance for the structure of the doorway state. The quoted data indicate that, in the energy range $E_\gamma \lesssim 25$ MeV, photoneutrons emitted from these nuclei originate directly from the doorway dipole state (semidirect effect). One can also see that allowance for the structure of the doorway state increases substantially the yield of semidirect photoneutrons, and this leads to a substantial increase in the theoretically predicted cross section for the respective (γ, n) reaction. The last circumstance is illustrated by Fig. 5. In this figure, the maximum of the cross section for the reaction $^{35}\mathrm{Ca}(\gamma, n)$ at an energy of $E_\gamma \sim 26$ MeV is associated with semidirect photoneutrons emitted by the $T_>$ component of the giant dipole resonance in ^{35}Ca.

Similar conclusions follow from an analysis of data based on calculations for photoproton reactions on calcium and tin isotopes having a high proton deficit and lying near the upper mass boundary of the isotopic chain. The photoproton spectra in Fig. 6 for the ^{56}Ca and ^{134}Sn nuclei are indicative of the dominance of the direct photoeffect in the energy range of $E_\gamma \lesssim 25$ MeV, this dominance becoming substantially stronger upon taking into account the structure of the doorway dipole state. Figure 7, which shows the cross sections for the reactions $^{56}\mathrm{Ca}(\gamma, p)$

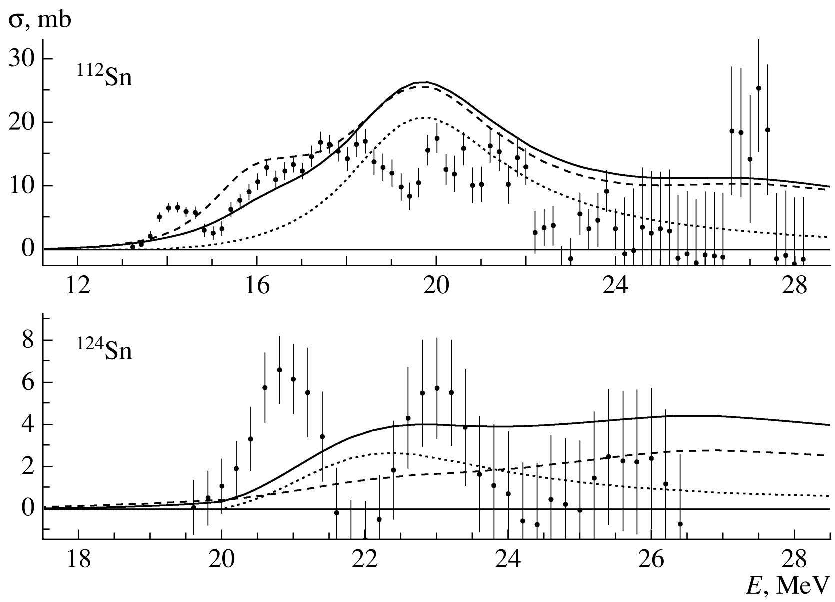

Fig. 12. Cross sections for the $(\gamma, p) + (\gamma, n + p)$ reactions on the tin isotopes ^{112}Sn and ^{124}Sn in the region around the giant dipole resonance. The displayed experimental data were borrowed from [45]. The notation for the curves is identical to that in Fig. 5.

and ^{134}Sn(γ, p), confirms that the disregard of the doorway-state structure leads to underestimated theoretical predictions for the (γ, p) cross sections in the case of target nuclei featuring a high proton deficit. This figure also shows that the cross section for the reaction ^{56}Ca(γ, p) receives a significant contribution from the emission of semidirect photoprotons in the $T_>$ reaction channel. No similar effect was observed for the ^{134}Sn nucleus. The reason for this is that the $T_>$ component of the giant dipole resonance is extremely small in this nucleus (see above).

7.3. Comparison with Experimental Data

A vast body of information about photoneutron reactions in the region of giant resonances ($E_\gamma \lesssim$ 30 MeV) was obtained in the 1960s and early 1970s upon detecting (moderated) neutrons that were emitted under the effect of bremsstrahlung and quasimonochromatic gamma radiation. The experimental photoneutron cross sections found by different authors frequently differ from one another not only in the details of the structure but also even in magnitude. This is not surprising since measurements performed with quasimonochromatic beams in Livermore (USA) and Saclay (France) do not have a sufficiently high energy resolution and since, in measurements employing beams of bremsstrahlung photons, one has to solve an unstable inverse problem in calculating the reaction cross section on the basis of the photoneutron yield curve. Moreover, the multiplicity sorting of photonucleon-reaction yields presents a difficult challenge in either case. The situation around photoproton data is even still worse. For medium-mass and medium-heavy nuclei, there are only fragmentary measurements of cross sections for (γ, p) reactions, since it is difficult to accumulate respective data in view of the suppression of the proton yield by the Coulomb barrier.

It should also be borne in mind that the measurements of the 1960s and the 1970s were performed only for beta-stable or rather long-lived beta-radioactive nuclei lying far from the mass boundaries of isotopic chains. This also constrains the possibilities for a comparison of theoretical and experimental data.

A comparison of the theoretical and experimental photonucleon cross sections is illustrated in Figs. 8–12. These figures show that, by and large, the results of the calculations are in fairly good agreement with experimental data (especially upon taking into account the uncertainties in the latter). In all of these figures, the experimental data are represented by points with bars corresponding to the estimated errors. The solid and dashed curves stand for the total reaction cross sections calculated, respectively, with and without allowance for the structure of the doorway dipole state. The dotted curves correspond to the contribution of the $T_>$ reaction component to the total reaction cross section calculated with allowance for the doorway-state structure.

An analysis of the quoted data shows that, in the region of beta-stable calcium and tin isotopes [apart from the description of the reactions ^{40}Ca(γ, n) and ^{124}Sn(γ, p)], the results of the calculations do not change substantially upon taking into account the structure of the doorway dipole state. This suggests that, in the region being considered, the emission of a major part of photonucleons occurs at the evaporation reaction stage. These data also illustrate the importance of taking into account the $T_>$ reaction channel in describing photoproton cross sections.

8. CONCLUSIONS

We will now list the basic results of the present study.

(i) We have formulated a new version of the previously developed combined photonucleon-reaction model. This version permits taking into account the effect of the isospin splitting and shell structure of the doorway dipole state on photonucleon reactions in moderately light and medium-mass nuclei at energies in the range of $E_\gamma \lesssim 30$ MeV.

(ii) Within this model, we have studied the dynamics of changes in the properties of photonucleon reactions upon going over from neutron-deficient to neutron-rich calcium and tin isotopes.

(iii) We have shown that, in describing photonucleon reactions near the lower and upper mass boundaries of the $^{35-56}$Ca and $^{102-134}$Sn isotopic chains, it is important to take into account the structure of the doorway dipole state, since nucleons belonging to the deficient fraction of the nucleus are predominantly emitted near these boundaries directly from the doorway state (semidirect photoeffect).

(iv) From the calculations performed in this study, it can be concluded that, in the region of beta-stable calcium and tin isotopes, photonucleons are predominantly emitted at the evaporation reaction stage.

(v) Our calculations have also demonstrated the importance of taking into account isospin effects in describing photonucleon reactions.

ACKNOWLEDGMENTS

This work was performed at the Department of Electromagnetic Processes and Interactions of Nuclei at the Skobeltsyn Institute of Nuclear Physics (Moscow State University) and was supported in part by the Russian Foundation for Basic Research (project no. 13-02-00124). We are deeply indebted to the physicist of this department for valuable consultations and enlightening discussions.

REFERENCES

1. N. Bohr, Nature **137**, 344 (1936).
2. J. M. Laget, Nucl. Phys. A **312**, 265 (1978).
3. J. M. Laget, in *Lecture Notes in Physics,* Vol. 137, Ed. by H. Arenhovel and A. M. Saruis (Springer, Berlin, 1981), p. 148.
4. G. E. Brown, *Unified Theory of Nuclear Models and Forces* (North-Holland, Amsterdam, 1967; Atomizdat, Moscow, 1970).
5. A. B. Migdal, *Theory of Finite Fermi Systems and Applications to Atomic Nuclei* (Nauka, Moscow, 1983, 2nd ed.; Interscience, New York, 1967, transl. 1st ed.).
6. B. Buck and A. D. Hill, Nucl. Phys. A **95**, 271 (1967).
7. S. Kamerdzhiev et al., Nucl. Phys. A **555**, 90 (1993).
8. S. P. Kamerdzhiev et al., Phys. Part. Nucl. **28**, 134 (1997).
9. V. A. Rodin and M. H. Urin, Phys. Rev. C **66**, 064608 (2002).
10. O. Bohr and B. R. Mottelson, *Nuclear Structure,* vol. 2: *Nuclear Deformations,* (Benjamin, New York, 1975; Mir, Moscow, 1977).
11. B. S. Ishkhanov and V. N. Orlin, Phys. Part. Nucl. **38**, 232 (2007).
12. J. S. Levinger, Phys. Rev. **84**, 43 (1951); Phys. Lett. B **82**, 181 (1979).
13. M. B. Chadwick et al., Phys. Rev. C **44**, 814 (1991).
14. G. Colò et al., Phys. Lett. B **485**, 362 (2000).
15. S. Shlomo and A. I. Sanzhur, Phys. Rev. C **65**, 044310 (2002).
16. M. L. Gorelik, I. V. Safonov, and M. H. Urin, Phys. Rev. C **69**, 054322 (2004).
17. M. L. Gorelik, B. A. Tulupov, and M. H. Urin, Phys. At. Nucl. **69**, 598 (2006).
18. M. L. Gorelik and M. H. Urin, Phys. At. Nucl. **69**, 1267 (2006).
19. C. K. Cline and M. Blann, Nucl. Phys. A **172**, 225 (1971).
20. C. K. Cline, Nucl. Phys. A **210**, 590 (1973).
21. E. Gadioli, E. Gadioli Erba, and P. G. Sona, Nucl. Phys. A **217**, 589 (1973).
22. J. Dobes and E. Beták, Nucl. Phys. A **272**, 353 (1976).
23. M. Blann, Phys. Rev. Lett. **27**, 337 (1971).
24. M. Blann, Phys. Rev. Lett. **28**, 757 (1972).
25. M. Blann and H. K. Vonach, Phys. Rev. C **28**, 1475 (1983).
26. M. Blann, Phys. Rev. C **54**, 1341 (1996).
27. M. Blann and M. B. Chadwick, Phys. Rev. C **57**, 233 (1998).
28. H. Feshbach, A. Kerman, and S. Koonin, Ann. Phys. (N. Y.) **125**, 429 (1980).

29. H. Nishioka, H. A. Weidenmüller and S. Yoshida, Ann. Phys. (N. Y.) **183**, 166 (1988).

30. A. J. Koning and M. B. Chadwick, Phys. Rev. C **56**, 970 (1997).

31. C. Kalbach, J. Phys. G **21**, 1519 (1995).

32. A. J. Koning and M. C. Duijvestijn, Nucl. Phys. A **744**, 15 (2004).

33. B. S. Ishkhanov and V. N. Orlin, Phys. At. Nucl. **72**, 410 (2009).

34. B. S. Ishkhanov and V. N. Orlin, Phys. At. Nucl. **74**, 19 (2011).

35. B. S. Ishkhanov and V. N. Orlin, Phys. At. Nucl. **76**, 30 (2013).

36. B. S. Ishkhanov and V. N. Orlin, Phys. At. Nucl. **66**, 659 (2003).

37. J. M. Akkermans and H. Gruppelaar, Phys. Lett. B **157**, 95 (1985).

38. J. Kopecky and M. Uhl, Phys. Rev. C **41**, 1941 (1990).

39. A. Gilbert and A. G. W. Cameron, Can. J. Phys. **43**, 1446 (1965).

40. B. Goulard and S. Fallieros, Can. J. Phys. **45**, 3221 (1967).

41. A. Veyssière et al., Nucl. Phys. A **227**, 513 (1974).

42. B. I. Goryachev et al., Sov. J. Nucl. Phys. **7**, 567 (1968).

43. G. J. O'Keefe et al., Nucl. Phys. A **469**, 239 (1987).

44. S. C. Fultz et al., Phys. Rev. **186**, 1255 (1969).

45. Yu. I. Sorokin et al., Sov. J. Nucl. Phys. **14**, 622 (1971).